

# Light-curve and spectral properties of ultra-stripped core-collapse supernovae leading to binary neutron stars

Takashi J. Moriya<sup>1,2\*</sup>, Paolo A. Mazzali<sup>3,4</sup>, Nozomu Tominaga<sup>5,6</sup>, Stephan Hachinger<sup>7</sup>, Sergei I. Blinnikov<sup>8,9,6</sup>, Thomas M. Tauris<sup>10,2</sup>, Koh Takahashi<sup>11</sup>, Masaomi Tanaka<sup>1,6</sup>, Norbert Langer<sup>2</sup>, and Philipp Podsiadlowski<sup>12,2</sup>

<sup>1</sup> *Division of Theoretical Astronomy, National Astronomical Observatory of Japan, National Institutes of Natural Sciences, 2-21-1 Osawa, Mitaka, Tokyo 181-8588, Japan*

<sup>2</sup> *Argelander Institute for Astronomy, University of Bonn, Auf dem Hügel 71, D-53121 Bonn, Germany*

<sup>3</sup> *Astrophysics Research Institute, Liverpool John Moores University, IC2, Liverpool Science Park, 146 Browlow Hill, Liverpool L3 5RF, UK*

<sup>4</sup> *Max Planck Institute for Astrophysics, Karl-Schwarzschild-Straße 1, D-85748 Garching, Germany*

<sup>5</sup> *Department of Physics, Faculty of Science and Engineering, Konan University, 8-9-1 Okamoto, Kobe, Hyogo 658-8501, Japan*

<sup>6</sup> *Kavli Institute for the Physics and Mathematics of the Universe (WPI), The University of Tokyo Institutes for Advanced Study, The University of Tokyo, 5-1-5 Kashiwanoha, Kashiwa, Chiba 277-8583, Japan*

<sup>7</sup> *Leibniz Supercomputing Centre (LRZ), Bavarian Academy of Sciences and Humanities, Boltzmannstraße 1, D-85748 Garching, Germany*

<sup>8</sup> *Institute for Theoretical and Experimental Physics, Bolshaya Cheremushkinskaya ulitsa 25, 117218 Moscow, Russia*

<sup>9</sup> *All-Russia Research Institute of Automatics, Sushchevskaya ulitsa 22, 127055 Moscow, Russia*

<sup>10</sup> *Max Planck Institute for Radio Astronomy, Auf dem Hügel 69, D-53121 Bonn, Germany*

<sup>11</sup> *Department of Astronomy, Graduate School of Science, The University of Tokyo, Hongo 7-3-1, Bunkyo, Tokyo 113-0033, Japan*

<sup>12</sup> *Department of Physics, University of Oxford, Denys Wilkinson Building, Keble Road, Oxford OX1 3RH, UK*

Accepted 2016 December 8. Received 2016 December 8; in original form 2016 August 25

## ABSTRACT

We investigate light-curve and spectral properties of ultra-stripped core-collapse supernovae. Ultra-stripped supernovae are the explosions of heavily stripped massive stars which lost their envelopes via binary interactions with a compact companion star. They eject only  $\sim 0.1 M_{\odot}$  and may be the main way to form double neutron-star systems which eventually merge emitting strong gravitational waves. We follow the evolution of an ultra-stripped supernova progenitor until iron core collapse and perform explosive nucleosynthesis calculations. We then synthesize light curves and spectra of ultra-stripped supernovae using the nucleosynthesis results and present their expected properties. Ultra-stripped supernovae synthesize  $\sim 0.01 M_{\odot}$  of radioactive  $^{56}\text{Ni}$ , and their typical peak luminosity is around  $10^{42} \text{ erg s}^{-1}$  or  $-16 \text{ mag}$ . Their typical rise time is 5 – 10 days. Comparing synthesized and observed spectra, we find that SN 2005ek, some of the so-called calcium-rich gap transients, and SN 2010X may be related to ultra-stripped supernovae. If these supernovae are actually ultra-stripped supernovae, their event rate is expected to be about 1 per cent of core-collapse supernovae. Comparing the double neutron-star merger rate obtained by future gravitational-wave observations and the ultra-stripped supernova rate obtained by optical transient surveys identified with our synthesized light-curve and spectral models, we will be able to judge whether ultra-stripped supernovae are actually a major contributor to the binary neutron star population and provide constraints on binary stellar evolution.

**Key words:** supernovae: general — supernovae: individual: SN 2005ek — supernovae: individual: SN 2010X — supernovae: individual: PTF10iuv — gravitational waves

## 1 INTRODUCTION

Multiplicity of massive stars plays an essential role in determining stellar structure at the time of their core collapse and thus their supernova (SN) properties (e.g., Langer 2012;

\* takashi.moriya@nao.ac.jp

Yoon 2015; Vanbeveren & Mennekens 2015; Marchant et al. 2016). In particular, the lack of hydrogen-rich layers in progenitors of stripped-envelope core-collapse SNe (i.e., Type IIb/Ib/Ic SNe), is often suggested to be caused by binary interaction (e.g., Wheeler & Livio 1985; Ensmann & Woosley 1988; Podsiadlowski, Joss, & Hsu 1992; Nomoto et al. 1994; Shigeeyama et al. 1994; Woosley et al. 1994; Bersten et al. 2012, 2014; Fremling et al. 2014; Ergon et al. 2015; Eldridge et al. 2015; Lyman et al. 2016a). The small typical ejecta mass estimated from light curves (LCs) of stripped-envelope SNe ( $\simeq 1 - 5 M_{\odot}$ , e.g., Sauer et al. 2006; Drout et al. 2011; Taddia et al. 2015; Lyman et al. 2016a), and nucleosynthetic signatures estimated from their spectral modeling (e.g., Jerkstrand et al. 2015), support progenitors with relatively small zero-age main-sequence (ZAMS) masses. The less massive ZAMS mass stars need to remove their hydrogen-rich envelopes with mass loss caused by binary interactions because of their inefficient radiation-driven wind (e.g., Podsiadlowski, Joss, & Hsu 1992; Nomoto, Iwamoto, & Suzuki 1995; Podsiadlowski et al. 2004b; Izzard, Ramirez-Ruiz, & Tout 2004; Yoon, Woosley, & Langer 2010; Eldridge, Langer, & Tout 2011; Benvenuto, Bersten, & Nomoto 2013; Lyman et al. 2016a; Eldridge & Maund 2016). It is also known that mass loss caused by binary interaction is essential to explain the observational ratio of stripped-envelope SNe to hydrogen-rich SNe (e.g., Eldridge, Izzard, & Tout 2008; Eldridge et al. 2013; Smith et al. 2011).

Some Type Ib/Ic SNe are known to have a much faster LC evolution than others. While typical Type Ib/Ic SNe reach their peak luminosity in  $\sim 20$  days (e.g., Drout et al. 2011; Prentice et al. 2016), rapidly-evolving SN LCs rise in less than  $\sim 10$  days and decline quickly on a similar timescale (e.g., Poznanski et al. 2010; Perets et al. 2010; Kawabata et al. 2010; Kasliwal et al. 2010; Ofek et al. 2010; Kasliwal et al. 2012; Drout et al. 2013, 2014; Inserra et al. 2015). The simplest way to interpret the rapid LC evolution of some Type Ib/Ic SNe is that their ejecta mass is much smaller than in the more slowly evolving SNe (see also, e.g., Kleiser & Kasen 2014; Drout et al. 2014; Tanaka et al. 2016). LC evolution becomes faster with smaller ejecta mass because of the smaller diffusion timescale. This is roughly proportional to  $(M_{\text{ej}}^3/E_{\text{ej}})^{1/4}$ , where  $M_{\text{ej}}$  is the ejecta mass and  $E_{\text{ej}}$  is the kinetic energy (e.g., Arnett 1982). The ejecta mass of rapidly-evolving SNe is typically estimated to be  $\sim 0.1 M_{\odot}$ , which is an order of magnitude smaller than that of typical Type Ib/Ic SNe (e.g., Poznanski et al. 2010; Kasliwal et al. 2012; Drout et al. 2013).

Type Ib/Ic SNe with rapidly-evolving LCs show diversity in their peak luminosities and spectra. SN 2002bj is among the first observed rapidly-evolving Type Ib/Ic SNe and among the brightest with its peak magnitude at around  $-18$  mag (Poznanski et al. 2010). Many rapidly-evolving SNe have their peak magnitudes at around  $-16$  mag with different spectral properties. One example of rapidly-evolving SNe in this luminosity range is so-called ‘‘Ca-rich gap transients.’’ They are optical transients whose peak luminosity lie between that of classical novae and SNe and they show strong Ca lines especially in the nebular phase (e.g., Kasliwal et al. 2012). Although they are called ‘‘Ca-rich’’ transients, they may not necessarily be Ca-rich. What

is indicated from their spectra is that they have a larger fraction of Ca to O than typical Type Ib/Ic SNe. Several progenitor scenarios have been suggested for these events (e.g., Perets et al. 2010; Kawabata et al. 2010), but their nature is not yet clear. There also exist rapidly-evolving SNe with similar luminosities to the Ca-rich gap transients but with very different spectral features such as SN 2005ek (Drout et al. 2013) and SN 2010X (Kasliwal et al. 2010). Another kind of rapidly-evolving SNe are SN 2002cx-like SNe, which are also known as Type Iax SNe; they are characterized by their strong Si and S features with relatively low photospheric velocities and by the wide peak luminosity range covering from  $\sim -14$  mag to  $\sim -19$  mag (e.g., Foley et al. 2013).

A number of possibilities have been suggested to obtain a small ejecta mass to explain the rapidly-evolving SNe, including some not related to the core collapse of massive stars (e.g., Moriya & Eldridge 2016; Dessart & Hillier 2015; Kashiyama & Quataert 2015; Kleiser & Kasen 2014; Shen et al. 2010; Moriya et al. 2010; Kitaura, Janka, & Hillebrandt 2006). In particular, Tauris et al. (2013); Tauris, Langer, & Podsiadlowski (2015) proposed an ‘‘ultra-stripped’’ core-collapse SN scenario to explain small ejecta masses. They showed that tight helium star–neutron star (NS) binary systems, presumably created in the common-envelope phase from high-mass X-ray binaries (Tauris & van den Heuvel 2006), can lead to the extreme stripping of the helium envelope and result in SNe with ejecta masses of the order of  $0.1 M_{\odot}$  or less. The SN ejecta mass from these systems is even less than those typically obtained in SN progenitors from the first exploding stars ( $\sim 1 M_{\odot}$ ) during binary evolution (e.g., Yoon, Woosley, & Langer 2010; Lyman et al. 2016a).

Several studies have investigated the observational properties of stripped-envelope SNe with ejecta larger than  $1 M_{\odot}$  coming from progenitors obtained from binary stellar evolution (e.g., Dessart et al. 2015). However, few LC and spectral studies have been carried out for ultra-stripped SNe. A previous study of ultra-stripped SNe (Tauris et al. 2013) only provided LC models. Because there are several proposed ways to make SNe with rapidly-evolving LCs, LC information is not sufficient to identify ultra-stripped SNe observationally. In addition, the  $^{56}\text{Ni}$  mass was treated as a free parameter in the previous study. In this paper, we investigate not only LCs but also spectral properties of ultra-stripped SNe by performing explosive nucleosynthesis calculations which provide an appropriate estimate for the  $^{56}\text{Ni}$  mass synthesized during the explosion, so that we can have a better understanding of their observational signatures and identify ultra-stripped SNe observationally.

Ultra-stripped SNe are closely connected to the formation of double NS systems. It was argued by Tauris et al. (2013); Tauris, Langer, & Podsiadlowski (2015) that *all* double NS systems formed in the Galactic disk (i.e., outside dense environments such as globular clusters) which are tight enough to merge within a Hubble time *must* have been produced from an ultra-stripped SN. Therefore, ultra-stripped SNe are related to sources of gravitational waves detected by LIGO (e.g., Abadie et al. 2010). In addition, double NS systems which merge are suggested to cause short gamma-ray bursts (Blinnikov et al. 1984; Paczynski 1986; Narayan, Paczynski, & Piran 1992) and *r*-process element nucleosynthesis (e.g., Rosswog et al.

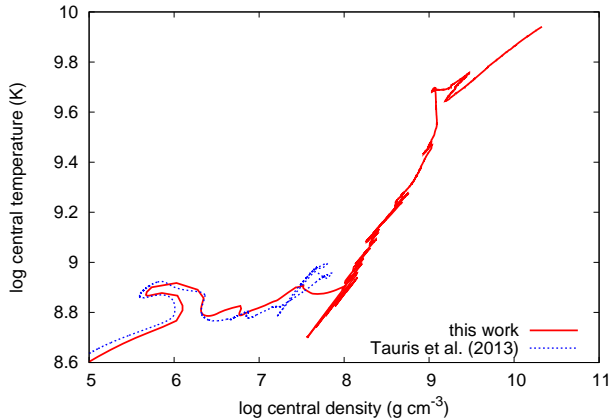


**Figure 1.** Evolution of the central density and temperature of our ultra-stripped SN progenitor obtained with MESA. We also present the central density and temperature evolution obtained by Tauris et al. (2013) with BEC.

1999; Argast et al. 2004; Hirai et al. 2015), possibly followed by a so-called “kilonova” (e.g., Metzger et al. 2010; Barnes & Kasen 2013; Tanaka & Hotokezaka 2013). However, to produce a double NS system a massive binary must survive two SN explosions. A binary system is likely to be disrupted by the first SN explosion because of a combination of sudden mass loss and a kick imparted to the newborn NS (Brandt & Podsiadlowski 1995). Ultra-stripped SNe, on the other hand, eject very little mass and are unlikely to have large NS kicks in general because of their rapid explosions (Podsiadlowski et al. 2004a; Suwa et al. 2015; Tauris, Langer, & Podsiadlowski 2015). Thus, ultra-stripped SNe avoid these two major obstacles in forming double NS systems and are therefore likely to produce systems which lead to merger events if the post-SN orbital period is short enough. Future constraints on the observed rate of ultra-stripped SNe can be directly compared to the double NS merger rate determined from gravitational wave observations (Tauris, Langer, & Podsiadlowski 2015). This can be used to verify their evolutionary connection. The merger rate of double NS systems will be known within a few years when LIGO/VIRGO reach full design sensitivity. We refer to Abadie et al. (2010); Berry et al. (2015); Abbott et al. (2016b) for detailed reviews on the expected merger rates.

This paper is organized as follows. Section 2 presents the numerical methods we adopt in our study. Our synthetic LC and spectral models are presented in Section 3. We compare our results with observations in Section 4. We discuss our results in Section 5 and conclude this paper in Section 6.

## 2 METHOD

### 2.1 Progenitor

We investigate the observational properties of explosions originating from the ultra-stripped SN progenitor presented in Tauris et al. (2013) (see also Tauris, Langer, & Podsiadlowski 2015). This is a typical model of ultra-stripped SNe. The total progenitor mass

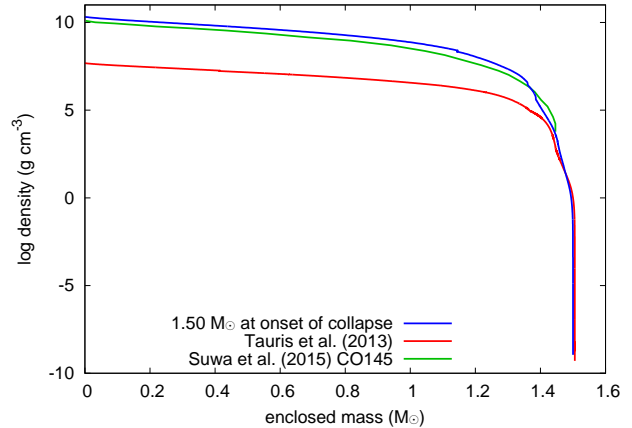


**Figure 2.** Progenitor density structure at core collapse. We also show the density structure from the model of Tauris et al. (2013) which is shortly after off-center oxygen ignition, some  $\sim 10$  years prior to core collapse. We show the density structure at the collapse from Suwa et al. (2015) from the progenitor having the same carbon+oxygen core mass of  $1.45 M_{\odot}$  as our model.

at explosion is  $1.50 M_{\odot}$  with a carbon+oxygen core of  $1.45 M_{\odot}$ . The helium ZAMS mass of the progenitor was  $2.9 M_{\odot}$ . Tauris et al. (2013) evolved the progenitor until shortly after the onset of off-center oxygen burning using the BEC binary stellar evolution code (Yoon, Woosley, & Langer 2010 and references therein). Although the remaining time to collapse is estimated to be about 10 years and the final progenitor mass does not change until the collapse, the density in the inner layers of the progenitor increases significantly in the remaining time. As the final density structure is critical for the explosive nucleosynthesis results, we need to follow the progenitor evolution until core collapse. The BEC code is not suitable for this.

In order to obtain a SN progenitor evolved until core collapse, we therefore used the public stellar evolution code MESA (Paxton et al. 2011, 2013, 2015). We used the same physical parameters as in the Tauris et al. (2013) BEC calculations in MESA. In particular, we used a mixing length parameter of 2 with a semiconvection efficiency parameter of 1. As the core mass is rather small, weak reactions play an important role in the evolution of the core approaching collapse (e.g., Takahashi, Yoshida, & Umeda 2013; Jones et al. 2013; Schwab, Quataert, & Bildsten 2015). Therefore we used the large nuclear network ‘‘mesa151.net’’ provided in MESA, which includes 151 nuclei up to  $^{65}\text{Ni}$  with important weak reactions such as electron capture by  $^{33}\text{S}$  and  $^{35}\text{Cl}$ . We stopped the calculation when the stellar core started to infall with a speed of  $1,000 \text{ km s}^{-1}$ .

First, we evolved a star starting from the helium ZAMS as is done by Tauris et al. (2013), but as a single star. Because the mass lost by the binary interactions like Roche-lobe overflow is known from the binary calculation of Tauris et al. (2013), we imposed their mass loss in our single-star evolution calculation. Thus, our single-star evolution calculation takes mass loss caused by binary stellar evolution into account in a simplified way. Tauris et al. (2013) obtained a  $1.50 M_{\odot}$  helium star with a carbon+oxygen core of  $1.45 M_{\odot}$  from a helium ZAMS

star of  $2.90 M_{\odot}$  which suffers from Roche-lobe overflow to a NS with initial orbital period of 0.1 days. We slightly increased the initial helium mass to  $2.949 M_{\odot}$  in order to obtain the same carbon+oxygen core mass after the core helium burning in our MESA calculation. The evolution of the central density and temperature is presented in Fig. 1. We find that the internal evolution of our progenitor is essentially the same as that in Tauris et al. (2013) up to the point they succeeded to follow. The star forms an Fe core and collapses as was presumed by Tauris et al. (2013); Tauris, Langer, & Podsiadlowski (2015). It is suggested that low-mass core-collapse SN progenitors experience violent silicon flashes shortly before the core collapse (Woosley & Heger 2015), but we do not find such a flash in our model. If such a flash occurs, it may result in a creation of a dense helium-rich circumstellar medium around the progenitor and the SN may be observed as Type Ibn (e.g., Moriya & Maeda 2016).

The final density structure of the progenitor at collapse is presented in Fig. 2. The abundance of the Fe-group elements sharply increases at an enclosed mass of  $1.35 M_{\odot}$ , while the electron fraction sharply decreases there. Thus, we estimate that the final iron-core mass at the time of collapse is  $1.35 M_{\odot}$ . This iron-core mass is comparable to that obtained recently by Suwa et al. (2015) ( $1.33 M_{\odot}$ ) from a progenitor model with a similar carbon+oxygen core mass as ours ( $1.45 M_{\odot}$ ). We compare our progenitor with that of Suwa et al. (2015) in Fig. 2. The internal structure of the collapsing models is similar. We also show for comparison the density structure obtained with the BEC code at a time  $\sim 10$  years prior to core collapse.

## 2.2 Nucleosynthesis

The collapsing progenitor described in the previous section was then used to follow the explosive nucleosynthesis. Numerical calculations of explosive nucleosynthesis were performed with the same numerical code as in previous studies of explosive nucleosynthesis in core-collapse SNe (e.g., Nakamura et al. 2001; Tominaga, Umeda, & Nomoto 2007). It is a one-dimensional explicit Lagrangian hydrodynamics code in which a piece-wise parabolic method is adopted (Colella & Woodward 1984). The  $\alpha$ -network is coupled with hydrodynamics and detailed nucleosynthesis calculations are performed as post-processing modelling. We used a reaction network including 280 isotopes up to  $^{79}\text{Br}$  (Table 1 in Umeda & Nomoto 2005).

## 2.3 Explosive hydrodynamics and light curves

Synthetic LCs were numerically obtained using the one-dimensional multi-group radiation hydrodynamics code STELLA (Blinnikov & Bartunov 1993; Blinnikov et al. 1998; Blinnikov & Sorokina 2004; Blinnikov et al. 2006; Baklanov, Blinnikov, & Pavlyuk 2005; Sorokina et al. 2015). STELLA has been used to model SN LCs of various kinds, including ultra-stripped SNe (Tauris et al. 2013). We take the progenitor structure above a mass cut and inject thermal energy at the bottom of the structure to initiate the explosion. The amount of thermal energy injected is  $E_{\text{ej}} + E_{\text{bind}}$ , where  $E_{\text{bind}}$  is the total binding energy of the

progenitor. We used the chemical composition obtained from explosive nucleosynthesis.

We show LC and spectral models obtained using two different mass cuts, at  $1.30 M_{\odot}$  and  $1.35 M_{\odot}$ , respectively. A mass-cut of  $1.35 M_{\odot}$  corresponds to the final iron-core mass of the progenitor model. Suwa et al. (2015) obtained a final NS baryonic mass of  $1.35 M_{\odot}$  from an explosion using the same carbon+oxygen core mass. Tauris et al. (2013) used a mass cut of  $1.30 M_{\odot}$ . Both the small Fe core mass of our progenitor model and simulations by Suwa et al. (2015) suggest that the mass cut is likely to be small.

## 2.4 Spectra

The spectral properties of ultra-stripped SNe have been investigated using the Monte Carlo spectral synthesis code developed by Mazzali & Lucy (1993). We refer to Mazzali & Lucy (1993); Lucy (1999); Mazzali (2000); Tanaka et al. (2011) for details. This code has been used for many SN spectral synthesis studies (e.g., Mazzali, Lucy, & Butler 1992; Mazzali et al. 1993; Mazzali, Iwamoto, & Nomoto 2000; Tanaka et al. 2011).

The code is applicable in early phases of SNe when a photosphere exists in the ejecta from where photons are assumed to be emitted with a blackbody spectrum. The code requires a density structure, abundances, position of the photosphere, and emerging SN luminosity to synthesize spectra. We used the average abundances of the models obtained from the nucleosynthesis calculations (Table 1) in our spectral modelling. We did not assume stratification of chemical elements in the SN ejecta because the ejecta mass is small and the ejecta are likely to be well mixed (e.g., Hachisu et al. 1991). We took the density structure and luminosity from STELLA. The spectral code assumes homologous expansion of the SN ejecta, which is satisfied in every model we present in this paper. A converging model is obtained by changing photospheric velocity and temperature in the spectral synthesis code.

Our models contain a large fraction of helium, and some rapidly-evolving SNe are of Type Ib. However, the code we mainly use does not include non-thermal excitation of helium which is essential in modelling helium features in SN spectra (e.g., Lucy 1991; Mazzali & Lucy 1998; Hachinger et al. 2012). We investigate the effect of non-thermal helium excitation using a code developed by Hachinger et al. (2012) and find that non-thermal excitation does not have a strong effect on the spectra we present in this study (Section 3.3.3).

## 3 RESULTS

### 3.1 Nucleosynthesis

We calculated explosive nucleosynthesis for three different explosion energies: 0.10, 0.25, and 0.50 B ( $1 \text{ B} \equiv 10^{51} \text{ erg}$ ). We investigated these small explosion energies based on the recent explosion simulations of ultra-stripped SNe by Suwa et al. (2015). They found that ultra-stripped SNe explode via the neutrino-driven mechanism and have small explosion energies, of the order of 0.1 B.

The results of our nucleosynthesis calculation for the

**Table 1.** Explosive nucleosynthesis results of the  $1.50 M_{\odot}$  model for different ejecta masses and explosion energies. Mass fractions at the end of the nucleosynthesis calculations are presented. The value in each column,  $a(x)$ , means that the corresponding mass fraction is  $a \times 10^x$ . The abundance estimated for SN 2005ek based on its peak spectrum (Drout et al. 2013) is also shown.  $T_{\max}$  is the maximum temperature reached during the explosive nucleosynthesis calculations.

element	$M_{\text{ej}} = 0.20 M_{\odot}$			$M_{\text{ej}} = 0.15 M_{\odot}$			SN 2005ek
	0.50 B	0.25 B	0.10 B	0.50 B	0.25 B	0.10 B	
He	2.4 (-1)	2.3 (-1)	2.2 (-1)	3.0 (-1)	2.9 (-1)	2.8 (-1)	-
C	4.3 (-2)	4.5 (-2)	4.7 (-2)	5.8 (-2)	6.0 (-2)	6.3 (-2)	2.0 (-2)
O	1.7 (-1)	1.8 (-1)	1.9 (-1)	2.3 (-1)	2.4 (-1)	2.5 (-1)	8.6 (-1)
Ne	5.2 (-2)	6.9 (-2)	7.9 (-2)	7.0 (-2)	9.2 (-2)	1.1 (-1)	-
Mg	2.3 (-2)	2.5 (-2)	2.6 (-2)	3.0 (-2)	3.4 (-2)	3.5 (-2)	8.2 (-2)
Si	5.1 (-2)	5.3 (-2)	6.0 (-2)	6.7 (-2)	7.0 (-2)	8.0 (-2)	2.5 (-2)
S	2.4 (-2)	2.5 (-2)	2.3 (-2)	3.2 (-2)	3.4 (-2)	4.0 (-2)	8.0 (-3)
Ca	3.9 (-3)	4.4 (-3)	5.1 (-3)	5.2 (-3)	5.8 (-3)	6.7 (-3)	1.2 (-3)
Sc	1.0 (-6)	1.0 (-6)	3.4 (-7)	4.3 (-7)	1.1 (-6)	3.8 (-7)	-
Ti	1.3 (-4)	7.2 (-5)	2.8 (-5)	1.3 (-4)	7.8 (-5)	3.1 (-5)	3.3 (-4)
V	3.2 (-6)	5.8 (-6)	2.4 (-6)	2.4 (-6)	6.6 (-6)	2.8 (-6)	-
Cr	2.7 (-4)	2.2 (-4)	1.9 (-4)	3.0 (-4)	2.6 (-4)	2.4 (-4)	3.3 (-4)
Mn	1.9 (-5)	2.6 (-5)	2.8 (-5)	2.4 (-5)	3.4 (-5)	3.8 (-5)	-
Fe	3.3 (-3)	4.3 (-3)	6.0 (-3)	4.3 (-3)	5.7 (-3)	8.0 (-3)	1.5 (-3)
Co	2.8 (-4)	4.0 (-4)	5.8 (-4)	3.7 (-4)	5.3 (-4)	7.7 (-4)	1.2 (-3)
$^{56}\text{Ni}$ mass	0.034 $M_{\odot}$	0.030 $M_{\odot}$	0.026 $M_{\odot}$	0.031 $M_{\odot}$	0.027 $M_{\odot}$	0.021 $M_{\odot}$	0.03 $M_{\odot}$
$T_{\max}/10^9$ K	14	12	11	7.5	6.6	6.0	-

case of  $E_{\text{ej}} = 0.25$  B is shown in Fig. 3. Table 1 shows the final average abundances in the ejecta for all energies and mass cuts we applied. One of the most important elements determining SN properties is the mass of  $^{56}\text{Ni}$  synthesised in the explosion. We find that the  $^{56}\text{Ni}$  masses range from 0.034 to 0.021  $M_{\odot}$  depending on explosion energy and mass cut (Table 1).

### 3.2 Light curves

Figure 4 shows the bolometric LCs of ultra-stripped SNe obtained in this study. After shock breakout, the bolometric LCs decline in the first 1 day owing to adiabatic cooling of the ejecta. Then, when the heating from  $^{56}\text{Ni}$  decay becomes dominant, the bolometric luminosity starts to increase again. The peak luminosity is approximately proportional to the initial  $^{56}\text{Ni}$  mass. In most cases, the peak luminosity does not exactly match that expected from a simple estimate based on Arnett (1982): it is larger by up to 50 per cent. The rise time and peak luminosity are consistent with those estimated in Tauris, Langer, & Podsiadlowski (2015) by using an analytic approach.

Figure 5 shows multi-color LCs of the same models with several Bessel filters (Bessell 1990). Optical LCs presented in Fig. 5 show some differences from the bolometric LCs. In particular, optical LCs show a first LC peak at times when bolometric LCs monotonically decline. This is a consequence of the cooling of the ejecta, which shifts the spectral peak to longer wavelengths as time goes on. Therefore, LCs in redder bands peak later.

In the models presented so far, we have used the chemical structure from the explosive nucleosynthesis modeling (cf. Fig. 3) and did not take into account the effect of mixing. To demonstrate the effect of mixing on the LCs, we show a LC in which  $^{56}\text{Ni}$  is uniformly mixed in the entire ejecta (Fig. 6). Because of the presence of  $^{56}\text{Ni}$  in the outer lay-

ers, heating by  $^{56}\text{Ni}$  in ejecta is more efficient early on and the rise time becomes shorter in the mixed model. However, at late phases, the gamma-rays in the outer layers are less trapped because of the smaller optical depth. Thus, the luminosity of the mixed model is less than that of the non-mixed model by about 50%. The decline rate after the LC peak is not strongly affected by mixing.

### 3.3 Spectra

#### 3.3.1 Peak spectra

We present synthetic spectra at maximum light in Fig. 7. We focus on this epoch's spectra because this is when ultra-stripped SNe are most likely to be observed. We compare these synthetic spectra with observations in Section 4.2.

Spectral features primarily depend on elemental abundances, photospheric temperature, and photospheric velocity. We used the mixed composition in Table 1 for our spectral modelling. Figure 8 shows the photospheric velocities and temperatures obtained by fitting the blackbody function to the spectral energy distributions (SEDs) obtained from STELLA. The photosphere here is defined as the location where the Rosseland mean optical depth is  $2/3$ . The circles in Fig. 8 represent the values in the converged spectral models of  $M_{\text{ej}} = 0.20 M_{\odot}$  and  $E_{\text{ej}} = 0.25$  B shown in Fig. 9. The photospheric temperature and velocity from the LC code and the spectral code match within 10 per cent.

Line shifts and broadening in spectra depend on the photospheric velocity. Because velocity is proportional to  $(E_{\text{ej}}/M_{\text{ej}})^{1/2}$ ,  $E_{\text{ej}}/M_{\text{ej}}$  is a good indicator of these properties. The models with  $E_{\text{ej}} = 0.25$  B have  $E_{\text{ej}}/M_{\text{ej}} \simeq 1$  B/ $M_{\odot}$ , which is similar to typical SNe Ia.

There are several notable features in our synthetic peak spectra. First of all, there are relatively strong Si II features, particularly Si II  $\lambda 6355$ . In some models, especially in the

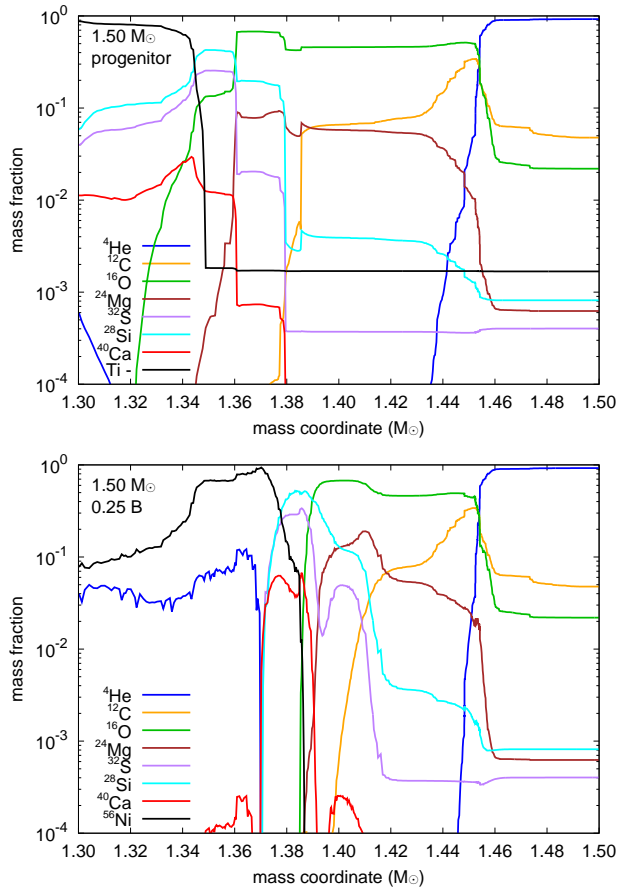


**Figure 3.** Chemical structure of the  $1.50 M_{\odot}$  progenitor at iron core collapse (top) and the result of our explosive nucleosynthesis calculation with the explosion energy  $0.25 B$  (bottom). The total abundance above Ti is plotted as a single line in the top panel (“Ti -”).

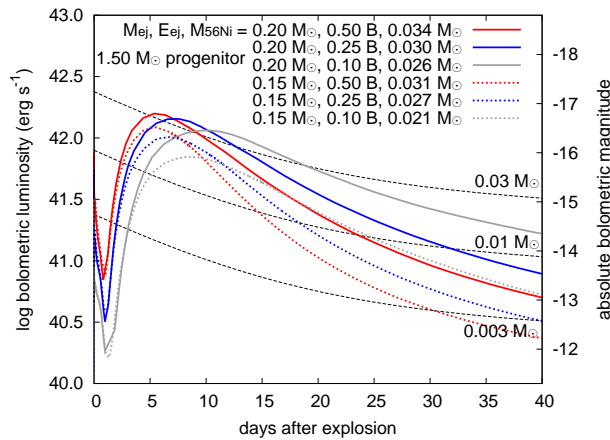


**Figure 4.** Bolometric LCs of ultra-stripped SNe. The thin dashed black lines show the total available energy from the nuclear decay of the indicated  $^{56}\text{Ni}$  masses.

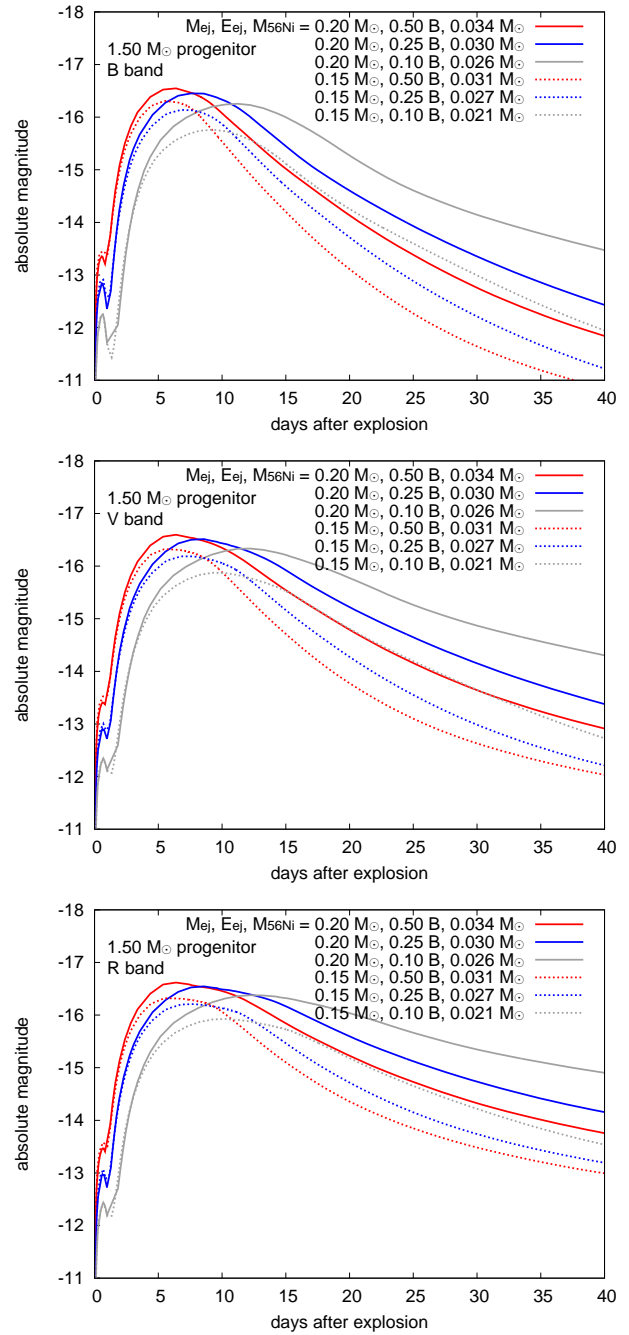


**Figure 5.** Multi-color LCs for the models shown in Fig. 4.

spectra with relatively small explosion energy, we can also see the C II  $\lambda 6582$  feature next to Si II  $\lambda 6355$ . We can find some S II features between  $5000 \text{ \AA}$  and  $6000 \text{ \AA}$ . O I  $\lambda 7774$  and Ca II IR triplet around  $8000 \text{ \AA}$  are also seen. The strong Ca feature in the  $M_{\text{ej}} = 0.15 M_{\odot}$  and  $E_{\text{ej}} = 0.50 B$  model is due to Ca ionization as is discussed in the next section.

### 3.3.2 Temporal evolution

We show the temporal evolution of our synthetic spectra with  $M_{\text{ej}} = 0.20 M_{\odot}$  and  $E_{\text{ej}} = 0.25 B$  in Fig. 9. We first present the spectrum at 0.5 days after the explosion, which

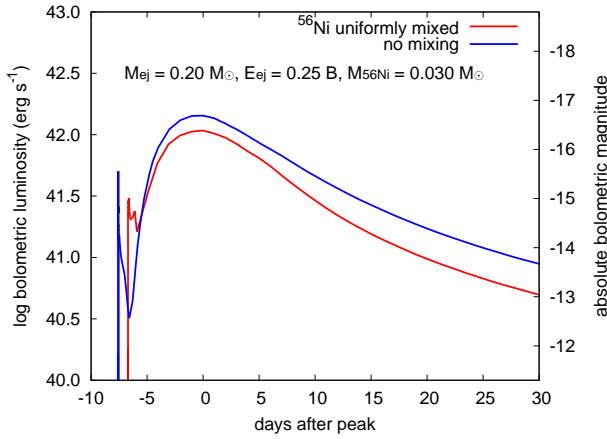


**Figure 6.** Bolometric LCs with and without  $^{56}\text{Ni}$  mixing. Bolometric LCs from the models with  $M_{\text{ej}} = 0.20 M_{\odot}$  and  $E_{\text{ej}} = 0.25 B$  are shown.

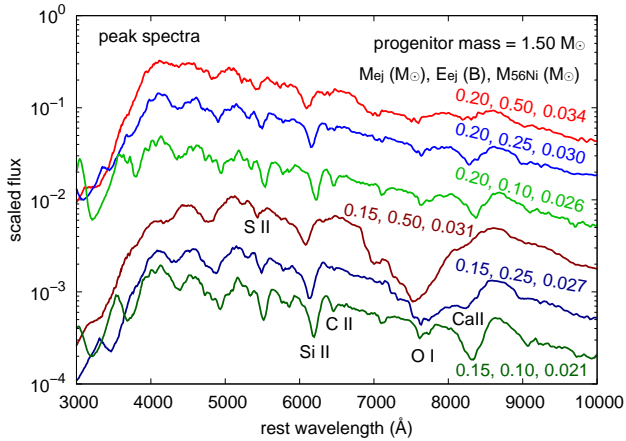


**Figure 7.** Synthetic spectra at bolometric LC peak for various models. The time of the bolometric LC peak is (from the top spectrum to the bottom) 5.3 days, 7.5 days, 10.2 days, 5.4 days, 6.8 days, and 8.2 days.

is still in the cooling phase after shock breakout (Fig. 4). This epoch roughly corresponds to the time when the optical LCs show the first peak (Fig. 5). The spectra during these very early epochs are similar to those of broad-line Type Ic SNe (SNe Ic-BL) because the photosphere is located in the high-velocity outer layers at that time (cf. Fig. 8).

Up to about 2.5 days after the explosion, a strong Ca absorption is observed between 7000 Å and 8000 Å. These broad features disappear by the time of LC peak, when the photospheric temperature becomes hot enough to change the Ca ionization level. The broad feature starts to appear again about 9 days after the explosion as the photosphere cools. There is no significant evolution in the spectra around LC peak, and the spectra quickly evolve to become nebular soon thereafter. A further study of the late-time spectra is beyond the scope of this paper.

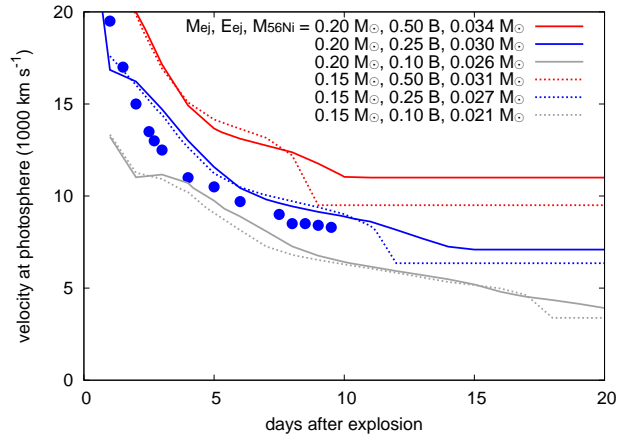
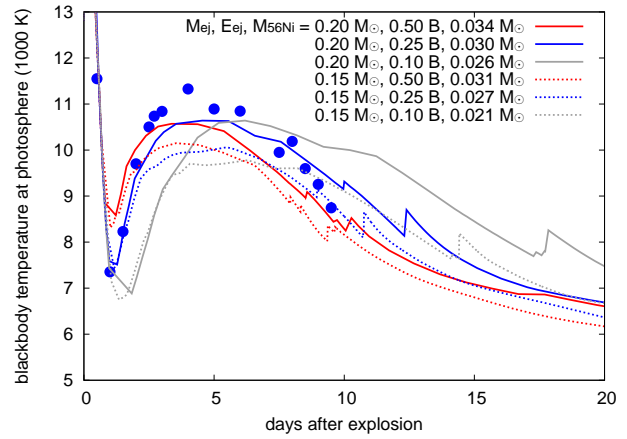


**Figure 8.** Photospheric temperature and velocity of the models from our STELLA LC calculations (solid and dotted lines). The filled circles indicate the results of the spectral synthesis code using the density structure from STELLA for the  $M_{\text{ej}} = 0.20 M_{\odot}$ ,  $E_{\text{ej}} = 0.25 B$  model. The synthesized spectra are presented in Fig. 9.

### 3.3.3 Helium features

Our progenitor contains about  $0.03 M_{\odot}$  of helium. This is close to the maximum helium mass that can be hidden without showing significant spectral features in relatively low-mass SNe Ib/Ic (about  $0.1 M_{\odot}$  of He Hachinger et al. 2012). It is important to judge whether ultra-stripped SNe from our progenitor are expected to be observed as Type Ib or Type Ic. However, the spectral synthesis code we have used so far does not take the non-thermal excitation required for helium excitation into account. Here, we show a spectral model where the effect of the non-thermal excitation is taken into account. The spectrum was computed with the spectral synthesis code described in Hachinger et al. (2012).

Figure 10 shows the spectrum including non-thermal excitation. In the optical range the spectrum is not strongly affected by non-thermal effects. Helium lines remain invisible except for the intrinsically strong  $\lambda 10830$  multiplet. Therefore, non-thermal excitation does not seem to cause significant changes to the spectra of ultra-stripped SNe.

The fact that He I remains practically invisible in our spectra, while  $0.1 M_{\odot}$  of helium could be detected in the SN Ib/Ic models of Hachinger et al. (2012), is not only due to

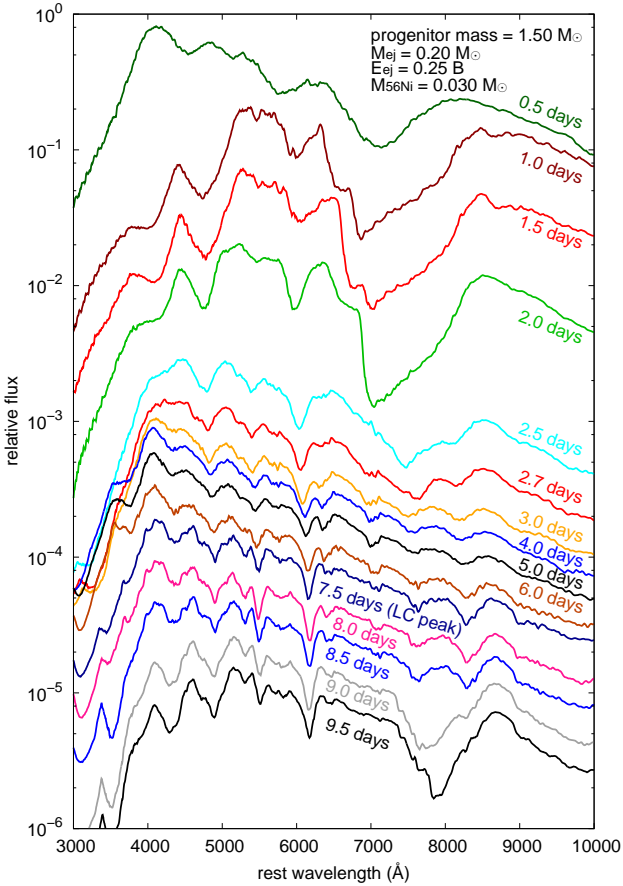


**Figure 9.** Temporal evolution of spectra for the model with  $M_{\text{ej}} = 0.20 M_{\odot}$  and  $E_{\text{ej}} = 0.25 B$ .

the somewhat smaller amount of  $^{56}\text{Ni}$  in our models. It can also be traced back to the fact that spectral temperatures are relatively high in our models, such that the non-thermal excitation effects rather result in a high ionization fraction (i.e. dominance of  $\text{He II}$ ) than in a large occupation number within  $\text{He I}$  excited states possibly generating lines. This is a situation somewhat similar to that of SLSNe (Mazzali et al. 2016).

## 4 COMPARISON WITH OBSERVATIONS

### 4.1 Light curves

Figure 11 shows a comparison between our synthetic LCs and observational data of rapidly-evolving SNe. The comparison is shown both in bolometric luminosity and in the  $B$  band. Overall, our LCs are consistent with faint rapidly-evolving SNe with peak luminosity of  $\sim 10^{42} \text{ erg s}^{-1}$  (i.e.,  $\sim -16 \text{ mag}$ ). Luminous SNe like SN 2002bj require more than  $0.1 M_{\odot}$  of  $^{56}\text{Ni}$  to explain the peak luminosity by  $^{56}\text{Ni}$ , which is inconsistent with the small amount of  $^{56}\text{Ni}$  ( $\sim 0.01 M_{\odot}$ ) we expect in our ultra-stripped SNe. Ultra-stripped SN LCs are consistent with those of rapidly-evolving faint SNe (e.g., SN 2010X, PS1-12bb, and SN 2008ha), the so-called Carich gap transients (e.g., PTF10iuv and SN 2005E), and SN 2005ek.

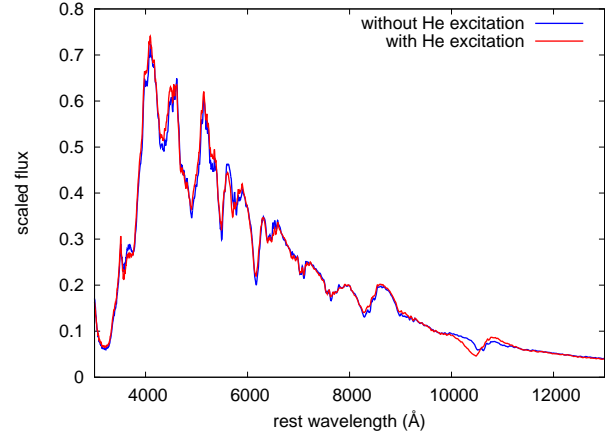


**Figure 10.** Synthetic spectra with with and without non-thermal helium excitation. The original model is the maximum light spectrum of the  $M_{\text{ej}} = 0.20 M_{\odot}$ ,  $E_{\text{ej}} = 0.25 B$  model with  $M_{\text{Ni}} = 0.025 M_{\odot}$ , which is also shown in Fig. 7.

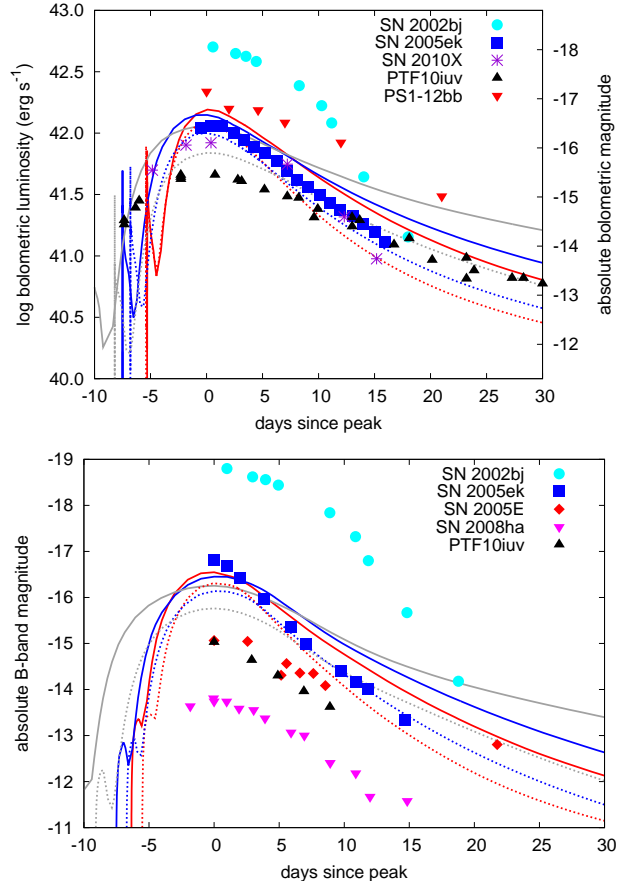


**Figure 11.** Comparison between our synthetic and observed bolometric (top) and  $B$ -band (bottom) LCs of rapidly-evolving SNe. These are from Drout et al. (2014) (PS1-12bb), Kasliwal et al. (2010) (SN 2010X), Drout et al. (2013) (SN 2005ek), Poznanski et al. (2010) (SN 2002bj), Kasliwal et al. (2012) (PTF10iuv), Perets et al. (2010) (SN 2005E), and Foley et al. (2009) (SN 2008ha).



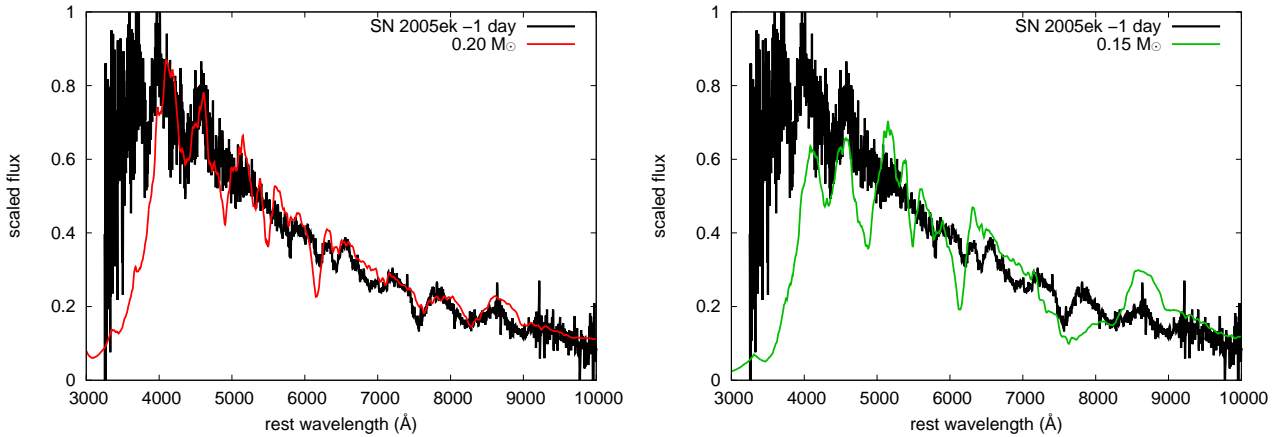


**Figure 12.** Comparison between our synthetic spectra and the observed spectrum of SN 2005ek one day before LC peak from Drout et al. (2013).

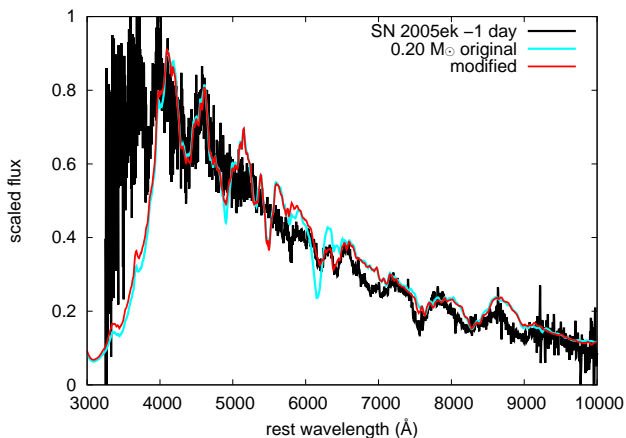


**Figure 13.** Synthetic spectrum for the  $M_{\text{ej}} = 0.20 M_{\odot}$  and  $E_{\text{ej}} = 0.25$  B model where the Si abundance is artificially reduced and the O abundance is artificially increased. The model provides a better match than the original one.

## 4.2 Spectra

We compare our models with observed near-LC-peak spectra of some rapidly-evolving SNe, i.e., SN 2005ek, two Ca-rich gap transients (PTF10iuv and SN 2005E), SN 2010X, SN 2002bj, and a SN 2002cx-like SN 2007qd. The observed spectra are taken from WISerEP<sup>1</sup> (Yaron & Gal-Yam 2012). We use synthetic spectra of 0.25 B for comparison, as there are no significant differences in spectral features (except for velocity) caused by the difference in the explosion energy in most spectra (Fig. 7). We correct the extinction of observed spectra by using the Galactic extinction law of Cardelli, Clayton, & Mathis (1989) assuming  $R_V = 3.1$ . The redshifts and extinctions applied are,  $z = 0.017$  and  $E(B - V) = 0.21$  mag for SN 2005ek (Drout et al. 2011),  $z = 0.02$  and  $E(B - V) = 0$  mag for PTF10iuv (Kasliwal et al. 2012),  $z = 0.0090$  and  $E(B - V) = 0.098$  mag for SN 2005E (Perets et al. 2010),  $z = 0.015$  and  $E(B - V) = 0.146$  mag

<sup>1</sup> <http://wiserep.weizmann.ac.il>

for SN 2010X (Kasliwal et al. 2010),  $z = 0.012$  and  $E(B - V) = 0$  mag for SN 2002bj (Poznanski et al. 2010), and  $z = 0.043$  and  $E(B - V) = 0.035$  mag for SN 2007qd (McClelland et al. 2010).

### 4.2.1 SN 2005ek

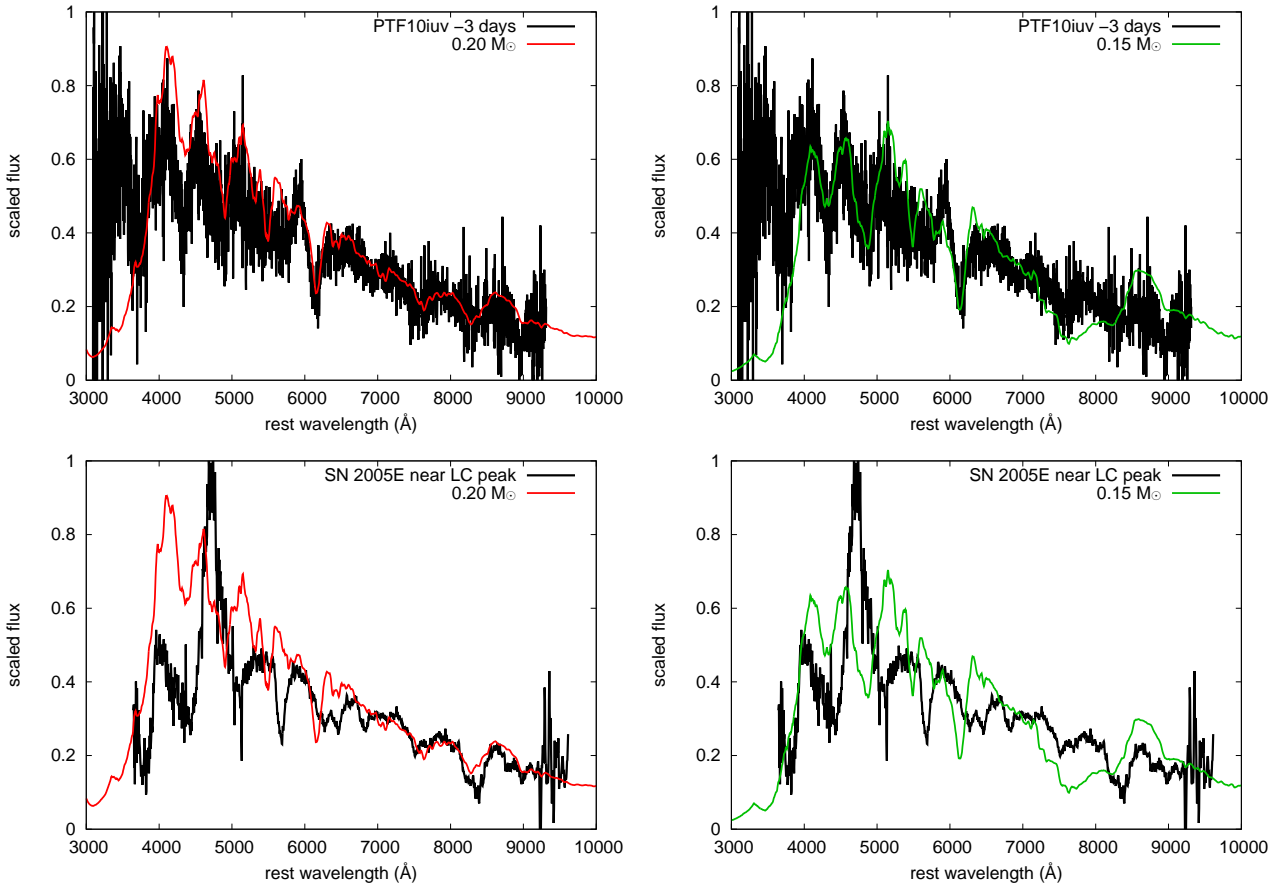
SN 2005ek was suggested to be a SN whose progenitor experienced extensive mass stripping by binary interactions (Drout et al. 2013). Its LC was shown to be consistent with our ultra-stripped SN model (Tauris et al. 2013), but the spectral properties have not yet been compared.

Figure 12 shows a comparison between synthetic spectra obtained from our ultra-stripped SN models and the spectrum of SN 2005ek one day before LC peak. Overall, continuum features and velocity shifts of the synthetic spectra match the observed spectrum well. In particular, the characteristic features in the red part of the spectrum of SN 2005ek, i.e., C I  $\lambda 6582$ , O I  $\lambda 7774$ , and Ca II IR triplet, are all well reproduced by the  $M_{\text{ej}} = 0.20 M_{\odot}$  model.

Our models predict stronger Si II features than seen in SN 2005ek. We find that we can obtain a better match by reducing the Si abundance from 0.053 to 0.003 and increasing the O abundance from 0.18 to 0.23 (Fig. 13). The strong Si features in the original ultra-stripped SN model may also be due to our assumption of fully-mixed ejecta. The average Si abundance used in the spectral modelling is around 0.05, while most of the outer layers have smaller fractions initially (Fig. 3). The smaller abundances may result in weaker Si features especially at early times. Thus, our assumption of full mixing may be too simplistic and SN 2005ek might have had a rather smaller degree of mixing. This may also explain the significant drop in flux below  $\sim 3500 \text{ \AA}$  in the model: a larger degree of mixing results in more Fe-group elements in the outer layers, leading to more line blocking which suppresses the NUV flux.

### 4.2.2 Ca-rich gap transients (PTF10iuv and SN 2005E)

Fig. 11 shows the LCs of two Ca-rich gap transients, PTF10iuv and SN 2005E. Their peak luminosity is slightly



**Figure 14.** Comparison between our synthetic spectra and the observed near-maximum spectra of the Ca-rich gap transients PTF10iuv (Kasliwal et al. 2012) and SN 2005E (Perets et al. 2010).

smaller than that of our ultra-stripped SNe, but the timescales of the LC evolution as well as the LC decline rates are similar. Efficient mixing in the ejecta may make the luminosity of our models slightly lower (Fig. 6), which motivates us to investigate their spectra.

Figure 14 shows a spectral comparison near peak luminosity. The spectral features including velocity shifts of PTF10iuv (top panels of Fig. 14) match our models well. Prominent features in PTF10iuv, such as Si II  $\lambda$ 6347, O I  $\lambda$ 7772, and Ca II  $\lambda$ 8542 are also well reproduced. We find relatively strong Si and Ca lines from our core-collapse progenitors because of the small values of the explosion energy and the progenitor mass. The overall color of PTF10iuv is consistent with our model. In summary, the LC and spectral properties of PTF10iuv are overall consistent with our ultra-stripped SN models.

On the other hand, our ultra-stripped SN spectral models are not consistent with the spectral features of the other Ca-rich gap transient, SN 2005E, very well, as shown in the bottom panels of Fig. 14. This indicates that there may be several kinds of progenitors for Ca-rich gap transients, of which some could be related to ultra-stripped SNe.

Ca-rich gap transients are typically found in remote locations from the center of their host galaxies (Kasliwal et al. 2012; Lyman et al. 2014, 2016b; Foley 2015). For example, PTF10iuv was 40 kpc away from the closest host galaxy

candidate (Kasliwal et al. 2012). This fact is used to relate Ca-rich gap transients to explosive events related to white dwarfs. However, Ca-rich transients are also found in the intergalactic space of merging galaxies (e.g., Foley 2015), where star formation is likely to take place (e.g., Mullan et al. 2011). Some massive stars are also known to exist very far from apparent star forming regions (e.g., Smith, Andrews, & Mauerhan 2016). It is also interesting to note that white dwarf mergers may actually end up as core-collapse SNe and could lead to SNe with similar properties to our ultra-stripped SNe (e.g., Nomoto & Iben 1985; Schwab, Quataert, & Kasen 2016). As we suggest here, Ca-rich gap transients can have different origin. Those found far from any host galaxy may be unrelated to ultra-stripped SNe. The faint nature of ultra-stripped SNe may also prevent them from being found in bright star-forming regions such as in galactic disks.

#### 4.2.3 SN 2010X

SN 2010X was a rapidly-evolving Type Ib SN. Its ejecta mass was estimated to be  $\sim 0.16 M_{\odot}$  and its  $^{56}\text{Ni}$  mass to be  $\sim 0.02 M_{\odot}$  (Kasliwal et al. 2010). These properties, as well as the LC evolution are similar to those of our ultra-stripped SNe (Fig. 11). SN 2010X had spectral characteristics similar

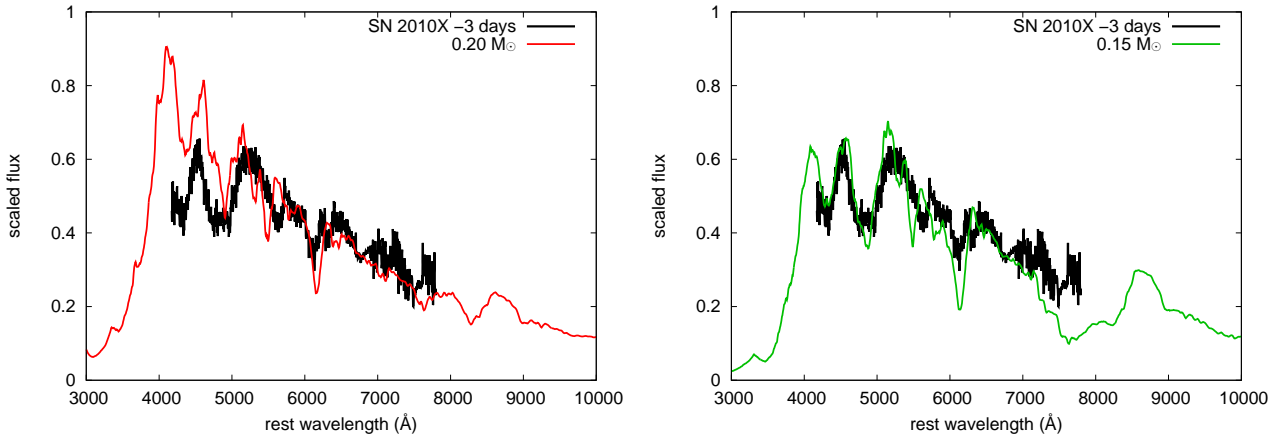


**Figure 15.** Comparison between our synthetic spectra and the spectrum of SN 2010X (Kasliwal et al. 2010) near LC peak.

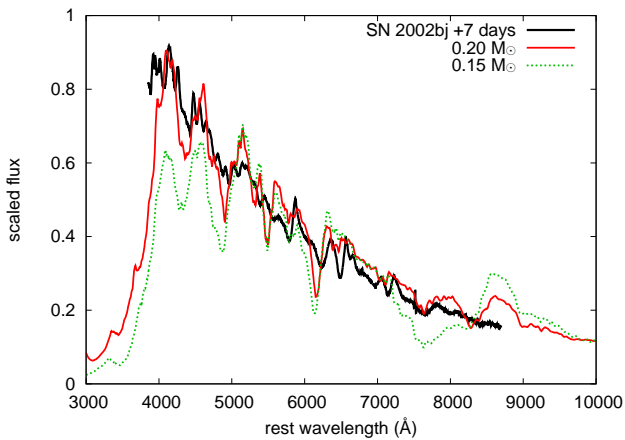


**Figure 16.** Comparison between our synthetic spectra at maximum and the earliest observed spectrum of SN 2002bj (Poznanski et al. 2010).

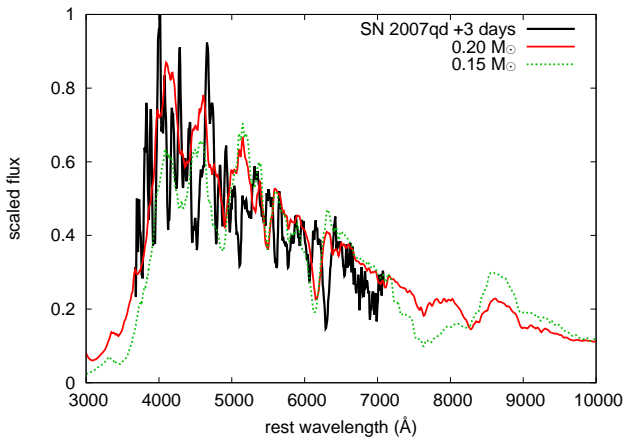


**Figure 17.** Comparison between our synthetic spectra at maximum and the observed spectrum of the SN 2002cx-like SN 2007qd near maximum (McClelland et al. 2010).

to SN 2002bj, which we discuss in the next section, but it was much fainter.

We compare our spectra with that of SN 2010X near LC peak in Fig. 15. Overall spectral features match well, especially the model with  $M_{\text{ej}} = 0.15 M_{\odot}$ . The Si II  $\lambda 6355$  is predicted to be slightly stronger, but a small reduction of the Si abundance or a slightly smaller degree of mixing could reduce the strength of this line as was discussed for SN 2005ek. Therefore, SN 2010X may also be related to ultra-stripped SNe.

#### 4.2.4 SN 2002bj

SN 2002bj was one of the first rapidly-evolving SNe to be reported (Poznanski et al. 2010). If SN 2002bj was powered by  $^{56}\text{Ni}$ , the amount of  $^{56}\text{Ni}$  required to explain its peak luminosity is  $0.15 - 0.25 M_{\odot}$  (Poznanski et al. 2010, see also Fig. 11). The amount of  $^{56}\text{Ni}$  required is much larger than what we expect from ultra-stripped SNe, and the  $^{56}\text{Ni}$  mass alone is comparable to the total ejecta mass expected from ultra-stripped SNe. This suggests that SN 2002bj is unlikely to be related to ultra-stripped SNe. Nonetheless, we show the comparison between our synthetic spectra and that of SN 2002bj. As expected, the match is not very good (Fig. 16).

#### 4.2.5 SN 2002cx-like (Type Iax) SNe

SN 2002cx-like SNe, which are often referred as Type Iax SNe, are a peculiar type of SN Ia with fainter peak luminosity. Their origin is still under discussion (e.g., Foley et al. 2016). Although many of them have peak magnitudes brighter than  $-17$  mag (see Foley et al. 2016 for a summary) and are thus too bright to be ultra-stripped SNe, some of them do have fainter peak luminosity (e.g., Stritzinger et al. 2014; McClelland et al. 2010). We take one faint SN 2002cx-like SN, SN 2007qd (McClelland et al. 2010), which is in the expected peak luminosity range for ultra-stripped SNe, and compare its spectrum at the peak luminosity with our synthetic spectra.

Figure 17 shows the comparison. SN 2002cx-like SNe have much lower velocities than our synthetic ultra-stripped

**Table 2.** Ultra-stripped SN candidates. An ‘✓’ or an ‘x’ indicate whether or not the SN properties match those expected of ultra-stripped SNe.

SN	LC	velocity	Si	Ca
SN 2005ek	✓	✓	✓	✓
PTF10iuv (Ca-rich gap)	✓	✓	✓	✓
SN 2005E (Ca-rich gap)	✓	x	x	✓
SN 2010X	✓	✓	✓	✓
SN 2002bj	x	x	x	x
SN 2007qd (02cx-like)	✓	x	✓	?

SN spectra. A low photospheric velocity is a commonly observed feature of faint SN 2002cx-like SNe. Our model with the smallest explosion energy (0.10 B) may have a photospheric velocity similar to that of some SN 2002cx-like SNe (Fig. 8), but it still seems to fail to reproduce crowded, unblended line features. In addition, the spectra of ultra-stripped SNe evolve quickly to the nebular regime, while the spectra of SN 2002cx-like SNe do not (e.g., Sahu et al. 2008; Foley et al. 2016).

### 4.3 Summary

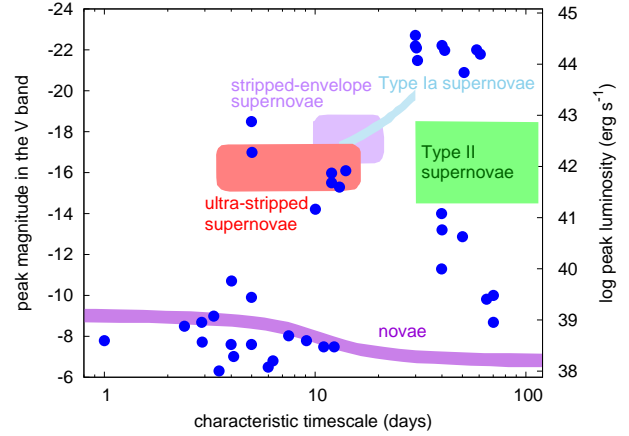
Table 2 summarizes the results of the comparison between our ultra-stripped SN models and possible observational counterparts. We find that SN 2005ek, PTF10iuv (Ca-rich gap transient), and SN 2010X match our synthetic ultra-stripped SN LCs and spectra.

## 5 DISCUSSION

### 5.1 Diversity

We have investigated the observational properties of an ultra-stripped SN explosion from a progenitor with a mass of  $1.50 M_{\odot}$ . Depending on the initial binary parameters and the helium ZAMS mass of the progenitor, the final total mass and core mass vary considerably (Tauris, Langer, & Podsiadlowski 2015). However, recent numerical simulations of explosions of ultra-stripped core-collapse SNe find that the explosion energy and the synthesized  $^{56}\text{Ni}$  mass do not change significantly among progenitors of different core masses (Suwa et al. 2015). Thus, the explosion energy and  $^{56}\text{Ni}$  mass values investigated in this paper are likely to remain similar even in different ultra-stripped SN progenitors. The low spread in the  $^{56}\text{Ni}$  masses found in our models suggests that the peak luminosity should be roughly similar in all ultra-stripped SNe, although the LC rise time can vary depending on the ejecta mass (Tauris, Langer, & Podsiadlowski 2015). In our one-dimensional model the  $^{56}\text{Ni}$  mass ejected depends on the mass cut, but Suwa et al. (2015) obtained similar  $^{56}\text{Ni}$  masses in their multi-dimensional explosion simulations. Thus, the spectral signatures we find in this study for a particular progenitor model are likely to be generic for ultra-stripped SNe.

A possible major source of diversity in ultra-stripped SN properties that may be caused by differences in their progenitors is their SN spectral type, which is determined

**Figure 18.** Characteristics of ultra-stripped SNe in the phase-space diagram of optical transients from Kulkarni (2012).

by the ejected helium mass. In the progenitor model we used in this study, there are  $0.03 M_{\odot}$  of helium in an ejected mass of  $0.15 - 0.20 M_{\odot}$ . Although helium features are not expected to be observed significantly in our model and we expect the explosion to be a SN Ic (Section 3.3.3), the helium mass as well as the ejecta mass can change depending on the initial binary configurations (Tauris, Langer, & Podsiadlowski 2015). Many progenitors are expected to have a helium mass above the critical helium mass ( $\sim 0.1 M_{\odot}$ , Hachinger et al. 2012) required to observe optical helium features (Tauris, Langer, & Podsiadlowski 2015), and thus may be observed as SNe Ib like SN 2010X.

To summarize, the expected luminosity range of ultra-stripped SNe is similar to that obtained with the model used in this paper. The diversity in SN ejecta masses caused by different progenitor systems could lead to diversity in the rise times of ultra-stripped SNe. We indicate the expected location of ultra-stripped SNe in the phase diagram of transients (e.g., Kulkarni 2012) in Fig. 18. It is likely that there is a smooth transition between ultra-stripped SNe and stripped-envelope SNe. The classical Type Ic SN 1994I, which had an ejecta mass of only  $1 M_{\odot}$  (e.g., Iwamoto et al. 1994; Sauer et al. 2006) may be an example of a SN Ic located between typical stripped-envelope SNe and ultra-stripped SNe. Also, the low-mass Type Ic SN 2007gr (Hunter et al. 2009; Mazzali et al. 2010) may be an even more extreme case.

### 5.2 Event rates

Based on our spectral analysis, we have shown that SN 2005ek and some of the Ca-rich gap transients, as well as SN 2010X, might be related to ultra-stripped SNe. The event rate of rapidly-evolving SNe including SN 2005ek, SN 2010X, and SN 2002bj are estimated to be at least 1-3 per cent of SNe Ia (Drout et al. 2013). The total event rate of the Ca-rich gap transients is estimated to be at least a few per cent of SNe Ia (Kasliwal et al. 2012; Perets et al. 2010). Given that a part of the transients included to estimate the two event rates actually correspond to ultra-stripped SNe, we can roughly estimate that the event rate for the ultra-stripped SNe based on SN observations is at

least a few per cent of SNe Ia. Because the volumetric rates of SNe Ia and SNe Ib/Ic are similar (e.g., Li et al. 2011), ultra-stripped SN rates are presumed to be at least a few per cent of SNe Ib/Ic. This rate corresponds to roughly 1 per cent of all core-collapse SNe including SNe II (Li et al. 2011) and matches the rough event rate estimate by Tauris et al. (2013) (0.1 – 1 per cent of core-collapse SNe). Further observational and theoretical studies to better estimate the event rate of ultra-stripped SNe are encouraged for their better comparison.

### 5.3 Synergy with gravitational-wave astronomy

Because ultra-stripped SNe are presumed to lead to double-NS systems, but not all double NS systems merge within a Hubble time, the observed rate of ultra-stripped SNe is expected to be larger than the rate of double-NS mergers. Furthermore, ultra-stripped SNe may also originate in binary systems with a white dwarf or a black hole accretor (Tauris et al. 2013). After the recent success in detecting gravitational wave signals from merging compact objects by advanced LIGO (Abbott et al. 2016a), it is expected that gravitational waves from merging double-NS systems will be detected in the near future, with advanced LIGO or other detectors like advanced VIRGO and KAGRA. Thus, it will soon be possible to obtain NS merger rate constraints from gravitational wave observations. This should place a lower limit to the rate of ultra-stripped SNe. Comparing the rates of ultra-stripped SNe and NS mergers, we will be able to test whether the ultra-stripped SN channel is actually the major path to form double-NS systems, and thus to constrain binary stellar evolution using gravitational waves.

The current constraints on the NS merger rate from LIGO is less than  $12600 \text{ Gpc}^{-3} \text{ yr}^{-1}$  (Abbott et al. 2016b). Assuming the Galactic core-collapse SN rate of  $\sim 0.01 \text{ yr}^{-1}$  and ultra-stripped SN fraction of 0.1 – 1 per cent in core-collapse SNe, we obtain an expected Galactic ultra-stripped SN rate of  $\sim 10^{-5} - 10^{-4} \text{ yr}^{-1}$ . If we adopt the Milky Way equivalent galaxy density of  $0.01 \text{ Mpc}^{-3}$  (Kopparapu et al. 2008), we expect an ultra-stripped SN rate of  $\sim 100 - 1000 \text{ Gpc}^{-3} \text{ yr}^{-1}$ . This is significantly lower than the current upper limit on the NS-NS merger rate from LIGO.

Finally, it should be noted that the distribution of eccentricities in current observations of NS-NS binaries (Martinez et al. 2015; Lazarus et al. 2016) supports the idea that ultra-stripped SNe are indeed the progenitors of the second SN in these systems, and that they often (but not always) result in small kicks. Out of 12 NS-NS systems, 9 have an eccentricity of less than 0.3. Moreover, even relatively small NS kicks of  $50 \text{ km s}^{-1}$  can result in post-SN eccentricities of more than 0.5, depending on the orbital period (Tauris et al. in preparation).

### 5.4 Observations of ultra-stripped SN progenitors

While it has been argued that the descendants of ultra-stripped SNe are often close pairs of NSs in binaries, it is much more difficult to find direct observational evidence for the progenitors of ultra-stripped SNe. Arguably, a fraction of high-mass X-ray binaries currently containing a NS and an OB-star will eventually evolve into double NS sys-

tems. Others will merge or become disrupted in the process. However, in between these two stages, the immediate progenitors of ultra-stripped stars would be found either as post-common envelope naked helium stars (Wolf-Rayet stars) or in an X-ray binary during the subsequent so-called Case BB Roche-lobe overflow. However, these phases are short lasting (especially the latter which is typically  $< 10^5 \text{ yr}$ , Tauris, Langer, & Podsiadlowski 2015) and thus chances of detecting these systems are small, even though the helium star is rather luminous ( $> 10^4 L_{\odot}$ ). One possible related observed system is Cygnus X-3 which is a close binary system with a NS or BH and a Wolf-Rayet star, but the mass of the Wolf-Rayet star (about  $10 M_{\odot}$ , Zdziarski, Miłkołajewska, & Belczyński 2013) is too high to correspond to an ultra-stripped SN progenitor.

## 6 CONCLUSIONS

We have presented synthetic LCs and spectral properties of ultra-stripped SNe. We evolved the ultra-stripped SN progenitor presented previously (Tauris et al. 2013) until core collapse, calculated its explosive nucleosynthesis, and then synthesized LCs and spectra. Our ultra-stripped SNe have explosion energies of  $1 - 5 \times 10^{50} \text{ erg}$  and ejecta masses of  $\sim 0.1 M_{\odot}$ . Explosive nucleosynthesis calculations show that they produce about  $0.03 M_{\odot}$  of  $^{56}\text{Ni}$ . We also found that ultra-stripped SNe have rise times of 5 – 10 days and their peak luminosity is  $\sim -16 \text{ mag}$  or  $10^{42} \text{ erg s}^{-1}$ .

Several types of transients have been found that have rise times and peak luminosities similar to those expected for ultra-stripped SNe. They show diverse spectral properties. We compared our synthetic spectra with those of rapidly-evolving transients showing LCs similar to those of our synthetic ultra-stripped SN LCs, and found that the spectra of SN 2005ek, some of so-called Ca-rich gap transients, and SN 2010X match reasonably well our synthetic ultra-stripped SN spectra. Not all Ca-rich gap transients have similar properties to our ultra-stripped SNe, indicating that this group of transients may include events with different origin. For example, the spectra of PTF10iuv are consistent with our ultra-stripped SN spectra, while those of SN 2005E are not. If all the transients above mentioned are actually from ultra-stripped SNe, the event rate of ultra-stripped SNe would be about one per cent of all stripped-envelope SNe.

It has been suggested that ultra-stripped SNe may be a major evolutionary path to form double-NS systems which could merge within a Hubble time and that double-NS systems left by ultra-stripped SNe may dominate the population of merging double-NS systems which is expected to be observed by GW observatories (Tauris et al. 2013; Tauris, Langer, & Podsiadlowski 2015). If this is true, we expect the NS merger rate to be comparable to or somewhat smaller than that of ultra-stripped SNe.

## ACKNOWLEDGMENTS

TJM thanks Yudai Suwa and Markus Kromer for helpful discussions. TJM is supported by Japan Society for

the Promotion of Science Postdoctoral Fellowships for Research Abroad (26-51) and by the Grant-in-Aid for Research Activity Start-up of the Japan Society for the Promotion of Science (16H07413). The work of S. Blinnikov on development of STELLA code is supported by Russian Science Foundation grant 14-12-00203. The work has also been supported by a Humboldt Research Award to PhP at the University of Bonn. Numerical computations were partially carried out on Cray XC30 and PC cluster at Center for Computational Astrophysics, National Astronomical Observatory of Japan. The numerical calculations were also partly carried out on Cray XC40 at Yukawa Institute for Theoretical Physics in Kyoto University. We made use of the Weizmann interactive supernova data repository - <http://wiserep.weizmann.ac.il>. This research has made use of the NASA/IPAC Extragalactic Database (NED) which is operated by the Jet Propulsion Laboratory, California Institute of Technology, under contract with the National Aeronautics and Space Administration.

## REFERENCES

- Abadie J., et al., 2010, *CQGra*, 27, 173001  
 Abbott B. P., et al., 2016a, *PhRvL*, 116, 061102  
 Abbott B. P., et al., 2016b, arXiv, arXiv:1607.07456  
 Argast D., Samland M., Thielemann F.-K., Qian Y.-Z., 2004, *A&A*, 416, 997  
 Arnett W. D., 1982, *ApJ*, 253, 785  
 Baklanov P. V., Blinnikov S. I., Pavlyuk N. N., 2005, *AstL*, 31, 429  
 Barnes J., Kasen D., 2013, *ApJ*, 775, 18  
 Benvenuto O. G., Bersten M. C., Nomoto K., 2013, *ApJ*, 762, 74  
 Berry C. P. L., et al., 2015, *ApJ*, 804, 114  
 Bersten M. C., et al., 2014, *AJ*, 148, 68  
 Bersten M. C., et al., 2012, *ApJ*, 757, 31  
 Bessell M. S., 1990, *PASP*, 102, 1181  
 Blinnikov S. I., Bartunov O. S., 1993, *A&A*, 273, 106  
 Blinnikov S. I., Novikov I. D., Perevodchikova T. V., Polnarev A. G., 1984, *SvAL*, 10, 177  
 Blinnikov S., Sorokina E., 2004, *Ap&SS*, 290, 13  
 Blinnikov S. I., Eastman R., Bartunov O. S., Popolitov V. A., Woosley S. E., 1998, *ApJ*, 496, 454  
 Blinnikov S. I., Röpke F. K., Sorokina E. I., Gieseler M., Reinecke M., Travaglio C., Hillebrandt W., Stritzinger M., 2006, *A&A*, 453, 229  
 Brandt N., Podsiadlowski P., 1995, *MNRAS*, 274, 461  
 Brott I., et al., 2011, *A&A*, 530, A115  
 Cardelli J. A., Clayton G. C., Mathis J. S., 1989, *ApJ*, 345, 245  
 Colella P., Woodward P. R., 1984, *JCoPh*, 54, 174  
 Dessart L., Hillier D. J., 2015, *MNRAS*, 447, 1370  
 Dessart L., Hillier D. J., Woosley S., Livne E., Waldman R., Yoon S.-C., Langer N., 2015, *MNRAS*, 453, 2189  
 Drout M. R., et al., 2014, *ApJ*, 794, 23  
 Drout M. R., et al., 2013, *ApJ*, 774, 58  
 Drout M. R., et al., 2011, *ApJ*, 741, 97  
 Eldridge J. J., Fraser M., Maund J. R., Smartt S. J., 2015, *MNRAS*, 446, 2689  
 Eldridge J. J., Fraser M., Smartt S. J., Maund J. R., Crockett R. M., 2013, *MNRAS*, 436, 774  
 Eldridge J. J., Izzard R. G., Tout C. A., 2008, *MNRAS*, 384, 1109  
 Eldridge J. J., Langer N., Tout C. A., 2011, *MNRAS*, 414, 3501  
 Eldridge J. J., Maund J. R., 2016, *MNRAS*, 461, L117  
 Ensmann L. M., Woosley S. E., 1988, *ApJ*, 333, 754  
 Ergon M., et al., 2015, *A&A*, 580, A142  
 Foley R. J., 2015, *MNRAS*, 452, 2463  
 Foley R. J., Jha S. W., Pan Y.-C., Zheng W. K., Bildsten L., Filippenko A. V., Kasen D., 2016, *MNRAS*, 461, 433  
 Foley R. J., et al., 2013, *ApJ*, 767, 57  
 Foley R. J., et al., 2009, *AJ*, 138, 376  
 Fong W., Berger E., 2013, *ApJ*, 776, 18  
 Fremling C., et al., 2014, *A&A*, 565, A114  
 Hachinger S., Mazzali P. A., Taubenberger S., Hillebrandt W., Nomoto K., Sauer D. N., 2012, *MNRAS*, 422, 70  
 Hachisu I., Matsuda T., Nomoto K., Shige-yama T., 1991, *ApJ*, 368, L27  
 Heger A., Langer N., Woosley S. E., 2000, *ApJ*, 528, 368  
 Hirai Y., Ishimaru Y., Saitoh T. R., Fujii M. S., Hidaka J., Kajino T., 2015, *ApJ*, 814, 41  
 Hunter D. J., et al., 2009, *A&A*, 508, 371  
 Inserra C., et al., 2015, *ApJ*, 799, L2  
 Iwamoto K., Nomoto K., Höflich P., Yamaoka H., Kumagai S., Shige-yama T., 1994, *ApJ*, 437, L115  
 Izzard R. G., Ramirez-Ruiz E., Tout C. A., 2004, *MNRAS*, 348, 1215  
 Jerkstrand A., Ergon M., Smartt S. J., Fransson C., Sollerman J., Taubenberger S., Bersten M., Spyromilio J., 2015, *A&A*, 573, A12  
 Jones S., et al., 2013, *ApJ*, 772, 150  
 Kashiyama K., Quataert E., 2015, *MNRAS*, 451, 2656  
 Kasliwal M. M., et al., 2012, *ApJ*, 755, 161  
 Kasliwal M. M., et al., 2010, *ApJ*, 723, L98  
 Kawabata K. S., et al., 2010, *Nature*, 465, 326  
 Kitaura F. S., Janka H.-T., Hillebrandt W., 2006, *A&A*, 450, 345  
 Kleiser I. K. W., Kasen D., 2014, *MNRAS*, 438, 318  
 Kopparapu R. K., Hanna C., Kalogera V., O’Shaughnessy R., González G., Brady P. R., Fairhurst S., 2008, *ApJ*, 675, 1459-1467  
 Kulkarni S. R., 2012, *IAUS*, 285, 55  
 Langer N., 2012, *ARA&A*, 50, 107  
 Lazarus P., et al., 2016, arXiv, arXiv:1608.08211  
 Li W., et al., 2011, *MNRAS*, 412, 1441  
 Lyman J. D., Bersier D., James P. A., Mazzali P. A., Eldridge J. J., Fraser M., Pian E., 2016a, *MNRAS*, 457, 328  
 Lyman J. D., Levan A. J., Church R. P., Davies M. B., Tanvir N. R., 2014, *MNRAS*, 444, 2157  
 Lyman J. D., Levan A. J., James P. A., Angus C. R., Church R. P., Davies M. B., Tanvir N. R., 2016b, *MNRAS*, 458, 1768  
 Lucy L. B., 1999, *A&A*, 345, 211  
 Lucy L. B., 1991, *ApJ*, 383, 308  
 Marchant P., Langer N., Podsiadlowski P., Tauris T. M., Moriya T. J., 2016, *A&A*, 588, A50  
 Martinez J. G., et al., 2015, *ApJ*, 812, 143  
 Mazzali P. A., 2000, *A&A*, 363, 705  
 Mazzali P. A., Iwamoto K., Nomoto K., 2000, *ApJ*, 545, 407  
 Mazzali P. A., Lucy L. B., 1993, *A&A*, 279, 447  
 Mazzali P. A., Lucy L. B., 1998, *MNRAS*, 295, 428

- Mazzali P. A., Lucy L. B., Butler K., 1992, *A&A*, 258, 399
- Mazzali P. A., Lucy L. B., Danziger I. J., Gouiffes C., Cappellaro E., Turatto M., 1993, *A&A*, 269, 423
- Mazzali P. A., Nomoto K., Patat F., Maeda K., 2001, *ApJ*, 559, 1047
- Mazzali P. A., Maurer I., Valenti S., Kotak R., Hunter D., 2010, *MNRAS*, 408, 87
- Mazzali P. A., Sullivan M., Pian E., Greiner J., Kann D. A., 2016, *MNRAS*, 458, 3455
- McClelland C. M., et al., 2010, *ApJ*, 720, 704
- Metzger B. D., et al., 2010, *MNRAS*, 406, 2650
- Modjaz M., Liu Y. Q., Bianco F. B., Graur O., 2015, *arXiv*, [arXiv:1509.07124](https://arxiv.org/abs/1509.07124)
- Moriya T. J., Eldridge J. J., 2016, *MNRAS*, 461, 2155
- Moriya T. J., Maeda K., 2016, *ApJ*, 824, 100
- Moriya T., Tominaga N., Tanaka M., Nomoto K., Sauer D. N., Mazzali P. A., Maeda K., Suzuki T., 2010, *ApJ*, 719, 1445
- Mullan B., et al., 2011, *ApJ*, 731, 93
- Nakamura T., Umeda H., Iwamoto K., Nomoto K., Hashimoto M.-a., Hix W. R., Thielemann F.-K., 2001, *ApJ*, 555, 880
- Narayan R., Paczynski B., Piran T., 1992, *ApJ*, 395, L83
- Nomoto K., Iben I., Jr., 1985, *ApJ*, 297, 531
- Nomoto K. I., Iwamoto K., Suzuki T., 1995, *PhR*, 256, 173
- Nomoto K., Thielemann F.-K., Yokoi K., 1984, *ApJ*, 286, 644
- Nomoto K., Yamaoka H., Pols O. R., van den Heuvel E. P. J., Iwamoto K., Kumagai S., Shigeyama T., 1994, *Nature*, 371, 227
- Ofek E. O., et al., 2010, *ApJ*, 724, 1396
- Paczynski B., 1986, *ApJ*, 308, L43
- Paxton B., Bildsten L., Dotter A., Herwig F., Lesaffre P., Timmes F., 2011, *ApJS*, 192, 3
- Paxton B., et al., 2013, *ApJS*, 208, 4
- Paxton B., et al., 2015, *ApJS*, 220, 15
- Perets H. B., et al., 2010, *Nature*, 465, 322
- Poznanski D., et al., 2010, *Science*, 327, 58
- Podsiadlowski P., Joss P. C., Hsu J. J. L., 1992, *ApJ*, 391, 246
- Podsiadlowski P., Langer N., Poelarends A. J. T., Rappaport S., Heger A., Pfahl E., 2004a, *ApJ*, 612, 1044
- Podsiadlowski P., Mazzali P. A., Nomoto K., Lazzati D., Cappellaro E., 2004b, *ApJ*, 607, L17
- Prentice S. J., et al., 2016, *MNRAS*, 458, 2973
- Rosswog S., Liebendörfer M., Thielemann F.-K., Davies M. B., Benz W., Piran T., 1999, *A&A*, 341, 499
- Sahu D. K., et al., 2008, *ApJ*, 680, 580-592
- Sauer D. N., Mazzali P. A., Deng J., Valenti S., Nomoto K., Filippenko A. V., 2006, *MNRAS*, 369, 1939
- Schwab J., Quataert E., Bildsten L., 2015, *MNRAS*, 453, 1910
- Schwab J., Quataert E., Kasen D., 2016, *arXiv*, [arXiv:1606.02300](https://arxiv.org/abs/1606.02300)
- Shen K. J., Kasen D., Weinberg N. N., Bildsten L., Scannapieco E., 2010, *ApJ*, 715, 767
- Shigeyama T., Suzuki T., Kumagai S., Nomoto K., Saio H., Yamaoka H., 1994, *ApJ*, 420, 341
- Smith N., Andrews J. E., Mauerhan J. C., 2016, *arXiv*, [arXiv:1607.01056](https://arxiv.org/abs/1607.01056)
- Smith N., Li W., Filippenko A. V., Chornock R., 2011, *MNRAS*, 412, 1522
- Sorokina E., Blinnikov S., Nomoto K., Quimby R., Tolstov A., 2015, *arXiv*, [arXiv:1510.00834](https://arxiv.org/abs/1510.00834)
- Stritzinger M. D., et al., 2014, *A&A*, 561, A146
- Suwa Y., Yoshida T., Shibata M., Umeda H., Takahashi K., 2015, *MNRAS*, 454, 3073
- Taddia F., et al., 2015, *A&A*, 574, A60
- Takahashi K., Yoshida T., Umeda H., 2013, *ApJ*, 771, 28
- Tanaka M., Hotokezaka K., 2013, *ApJ*, 775, 113
- Tanaka M., Mazzali P. A., Stanishev V., Maurer I., Kerzendorf W. E., Nomoto K., 2011, *MNRAS*, 410, 1725
- Tanaka M., et al., 2016, *ApJ*, 819, 5
- Tauris T. M., Langer N., Moriya T. J., Podsiadlowski P., Yoon S.-C., Blinnikov S. I., 2013, *ApJ*, 778, L23
- Tauris T. M., Langer N., Podsiadlowski P., 2015, *MNRAS*, 451, 2123
- Tauris T. M., van den Heuvel E. P. J., 2006, in Lewin W., van der Klis M., eds, *Compact Stellar X-ray Sources*. Cambridge Univ. Press, Cambridge, p. 623
- Tominaga N., Umeda H., Nomoto K., 2007, *ApJ*, 660, 516
- Umeda H. & Nomoto K., 2005, *ApJ*, 619, 427
- Vanbeveren D., Mennekens N., 2015, *arXiv*, [arXiv:1508.04282](https://arxiv.org/abs/1508.04282)
- Wanajo S., Nomoto K., Janka H.-T., Kitaura F. S., Müller B., 2009, *ApJ*, 695, 208
- Weisberg J. M., Nice D. J., Taylor J. H., 2010, *ApJ*, 722, 1030
- Wheeler J. C., Levreault R., 1985, *ApJ*, 294, L17
- Woosley S. E., Eastman R. G., Weaver T. A., Pinto P. A., 1994, *ApJ*, 429, 300
- Woosley S. E., Heger A., 2015, *ApJ*, 810, 34
- Yaron O., Gal-Yam A., 2012, *PASP*, 124, 668
- Yoon S.-C., 2015, *PASA*, 32, e015
- Yoon S.-C., Woosley S. E., Langer N., 2010, *ApJ*, 725, 940
- Zdziarski A. A., Mikołajewska J., Belczyński K., 2013, *MNRAS*, 429, L104